Analysis of Deterioration Characteristics in Oil-immersed Insulation Pressboard with Different Durations of Aging Based on an Image-processing Method

Yongqiang Wang,* Ruoyu Fei, Changhui Feng, and Jing Shang

Insulation pressboard samples were obtained by thermal aging (according to Montsinger's formula, at 130 °C, the pressboard is heated for 0 to 32 days) and discharge experiments. SEM images of samples were analysed. Image segmentation was applied to calculate the fibre width, cross-sectional porosity, and carbon-trace area. Inter-layer fibre models were established to observe fibre morphology using 3-D reconstruction. The initial discharge voltage decreased with age, and the discharge amounts increased. After 16 days of aging, the fibre width had decreased to between 68.1% and 81.8% of unaged pressboard. As the aging increased, cellulose hydrogen bonds were broken, which affected the expansion of interlayer pores, increasing the porosity of the pressboard. After 32 days of aging, the porosity increased to 2.38 times that of a new pressboard. In addition, the longer the aging, the larger the area of carbon marks caused by the discharge breakdown. With the aggravation of thermal aging, the insulating property of pressboard decreased due to the decrease of fibre width and increase of porosity that further accelerated the damage to the fibre structure. It was concluded that the fibre width and porosity could be used as criteria to judge the degradation of pressboard.

Keywords: Thermal aging; Oil-immersed insulation pressboard; Microscopic morphology; Image segmentation; Fibre

Contact information: Hebei Provincial Key Laboratory of Power Transmission Equipment Security, Department of Electrical Engineering, North China Electric Power University, Baoding 071003, China;
** Corresponding author: qianghd@126.com*

INTRODUCTION

Insulation paper is a solid organic insulation material that is widely used in power transformers. However, during long-term transformer operations, high-temperature exposure causes insulation paper to become thermally cracked, and the paper gradually deteriorates (Darveniza *et al.* 1992; Lundgaard *et al*. 2004). To address this concern, extensive research has been conducted (Joshi and Bhanot 2005; Joshi *et al.* 2006; Wang *et al.* 2018a). Simultaneously, studies have shown that cellulose, the main component of pressboard, undergoes a depolymerisation reaction and an elimination reaction under the action of heat. These reactions produce many derivatives, and the resulting derivatives will lead to other more complex chemical reactions, resulting in continuous changes in the fibre structure. When judging the aging state of insulating paper, researchers initially measure the insulation paper tensile strength (TS) to determine its condition. Secondly, people also use the degree of polymerisation as a parameter indicative of aging (Emsley *et al.* 1997). With improvement in the accuracy of observation equipment, researchers have begun to use atomic force microscopy (AFM), scanning electron microscopy (SEM), and other

methods to study the aging state of insulating oil paper from a microscopic perspective. Through analysing insulating paper of varying age, Carrascal *et al.* (2018) obtained information on the kinetics of their aging degradation. Li *et al.* (2017) studied the changes of moisture, acid value, and furfural in insulating grease paper under thermal aging.

Image processing includes image enhancement and image segmentation, including wavelet transform (Kim *et al*. 2016), threshold method (Otsu *et al*. 1979), boundary detection method, area method, *etc.* At present, image processing technology is widely used. Researchers use mature image processing software or mathematical function software for image processing. They are involved in the study of insulators (Pirie *et al*. 2020) and transformers (Mariprasath and Kirubakaran 2018), but they are rarely used in the analysis of insulating pressboard microstructure. Liao *et al.* (2008, 2011), by analysing SEM images, found that thermal aging resulted in cracks at the fibre surface, fibre peeling, cracking, pitting during discharge. Yan *et al.* (2011, 2012) used AFM to analyse the molecular chain changes on the microscopic surface of fibres. It was found that the oil-immersed paper surface consists of droplets and crystalline solids, which develop over time as damage accumulates. These conclusions are mainly through direct observation of SEM images. That is, there is insufficient statistical information available, and more clear data are needed to reach conclusions.

In this study, SEM images of pressboard under different aging conditions were observed using image processing techniques. Meanwhile, a three-dimensional model of the fibre was established to analyse the internal fibre morphology of the insulating pressboard. The microscopic information before and after breakdown of the needle plate discharge model at different thermal aging stages was calculated. The main purpose was to obtain data related to the deterioration of the pressboard. Through the calculation of the data, the deterioration degree of the pressboard can be quantitatively evaluated, and the trends of micro-morphology feature quantity changes, such as fibre width and porosity, can be further analysed. The present work will provide data support and new research ideas for further research on the long-term use ability and value of pressboard.

EXPERIMENTAL

Design of Discharge Experiment of Insulation Pressboard

Samples at these different states were prepared before discharge testing. Standard insulation pressboard, 80 mm × 80 mm × 2 mm, and Karamay 25# transformer oil (Sinopec Lubricants Co., Ltd., Beijing, China) were used for this experiment. The insulating pressboard was made from ultra-high voltage transformer pressboard (Weidmann Electrical, Co., Ltd., Rapperswil-Jona, Switzerland) comprised mainly of wood pulp, which is primarily composed of cellulose, hemicellulose, and lignin. The density of the insulation paper used in this paper was 1.20 g/cm^3, the relative dielectric constant (before the experiment) was 3.59, and the insulation resistivity was 6.25 × 1013 Ω·m. The specific preparation process was as follows: an appropriate amount of pressboard and Karamay 25# transformer oil were placed in a vacuum drying oven at 90 ℃ and 50 Pa to dry for 24 h to remove water and air bubbles in the pressboard. Subsequently, the temperature was adjusted to 80 ℃, the pressboard was immersed in transformer oil, and vacuum impregnated for 12 h. The pre-treated oil and pressboard were blended at a mass ratio of 10:1 and subjected to accelerated aging at 130 ℃ (Wang *et al.* 2018b). The aging time was calculated using Montsinger's rule (Tu *et al.* 2016; Zhou *et al.* 2017),

$$T = T_0 e^{-\alpha(\theta - C)} \quad (1)$$

where C is the reference operating temperature (80 °C) of the insulating material, T_0 is the insulation life at the reference working temperature, θ is the actual working temperature of the insulating material (130 °C), T is the insulating life at the actual working temperature, and α is the thermal aging coefficient. In Chinese transformers, the thermal aging factor α is generally 0.1155. In this paper, considering the safety and efficiency of the experiment, selected pressboards were aged for 0 days, 2 days, 4 days, 8 days, 16 days, and 32 days, which are equivalent to the normal operation of the transformer for 0 years, 1.77 years, 3.53 years, 7.06 years, 14.12 years, and 28.24 years, respectively. After aging, the insulation pressboard was immersed in filtered and purified new oil for two days. Subsequently, the vacuum was extracted three times to fully aspirate the aged oil in the pressboard.

The discharge device consisted of a needle electrode with a length of 30 mm, a width of 1 mm, a tip curvature of 30°, and a brass plate with a width of 100 mm and a thickness of 20 mm. The whole experimental platform is shown in Fig. 1. It was comprised of a booster console, an experimental transformer, a protective resistor, a coupling capacitor, and a smooth aluminium conductor. Among them, the non-corona testing transformer was a YDTW 50/250-type oil-immersed transformer (Wang *et al.* 2019a).

The experiment was conducted using the constant voltage method. When testing with high voltages, pressure measurement was completed at a step rate of 1 kV/s. When the signal of the PD tester was stable, the voltage was stabilised for 5 min, and this voltage value was noted as the initial discharge voltage U_0. It was understood that $U = 1.2U_0$ and U was applied as a constant voltage on the pressboard until the pressboard broke down.

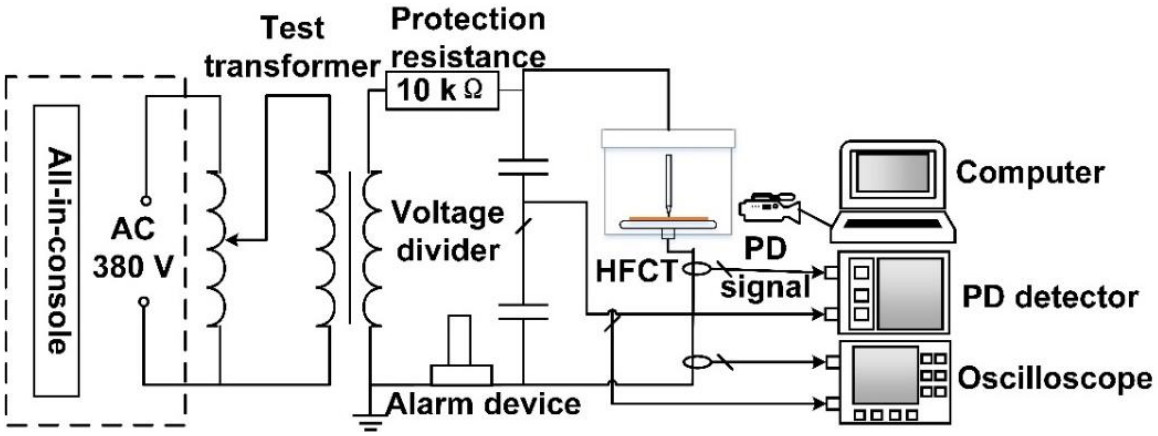

Fig. 1. Discharge experimental platform

SEM Image Processing

The objective guiding the extraction of the fibre profile from the SEM image was the identification of the dividing point between the fibre profile and the background, and the dividing points between fibres. First, the image was converted into a greyscale image. After calculating the histogram of the greyscale image (Fig. 2b), the OTSU algorithm was used to separate the fibres from the background.

The OTSU (Du *et al.* 2019) functions by using the characteristics of the grey image to divide the picture into two parts: the background and the foreground. In the binarized

image, the segmentation threshold between the fibre and background is T, the ratio of the number of pixels in the fibre N_0 to the entire image is ω_0, the average greyscale is μ, the ratio of the number of pixels N_1 in the background to the total pixels is ω_1, the background average greyscale is μ_1, the classes square error is g, the pixel points of the image length and width are respectively M and N, whereby:

$$\begin{cases}\omega_0 = N_0/(MN) \\ \omega_1 = N_1/(MN)\end{cases} \tag{2}$$

$$\begin{cases} N_0 + N_1 = MN \\ \omega_0 + \omega_1 = 1 \\ \mu = \omega_0\mu_0 + \omega_1\mu_1 \\ g = \omega_0(\mu_0 - \mu)^2 + \omega_1(\mu_1 - \mu)^2 \end{cases} \tag{3}$$

If the g was maximized and the threshold T was the required value, then the first divided image $f(x,y)$ was obtained.

After the fibre and background segmentation were divided, the watershed image segmentation algorithm based on top-hat transformation was selected for the second segmentation, and improved the algorithm using multi-structure element morphology.

The second segmentation was performed using a watershed segmentation algorithm:

$$grad\big(f(x,y)\big) = \{[f(x,y) - f(x-1,y)]^2 + [f(x,y) - f(x,y-1)]^2\}^{\frac{1}{2}} \tag{4}$$

$$G(x,y) = grad\big(f(x,y)\big) \tag{5}$$

$$G' = G \circ \mathrm{b} = G \ominus b \oplus b \tag{6}$$

where $\ominus$ is the corrosion operation symbol, $\oplus$ is the expansion symbol, and b is composed of three basic structural elements:

$$b_1 = \begin{bmatrix}0 & 0 & 0\\ 1 & 1 & 1\\ 0 & 0 & 0\end{bmatrix} \quad b_2 = \begin{bmatrix}0 & 1 & 0\\ 0 & 1 & 0\\ 0 & 1 & 0\end{bmatrix} \quad b_3 = \begin{bmatrix}0 & 1 & 0\\ 1 & 0 & 1\\ 0 & 1 & 0\end{bmatrix} \tag{7}$$

Substituting b_1, b_2, and b_3 into Eq. 4 to obtain G'_1, G'_2, and G'_3 and assigning different weights α_1, α_2, and α_3 to obtain G', gives the final fibre extraction image:

$$G' = \alpha_1 G'_1 + \alpha_2 G'_2 + \alpha_3 G'_3 \tag{8}$$

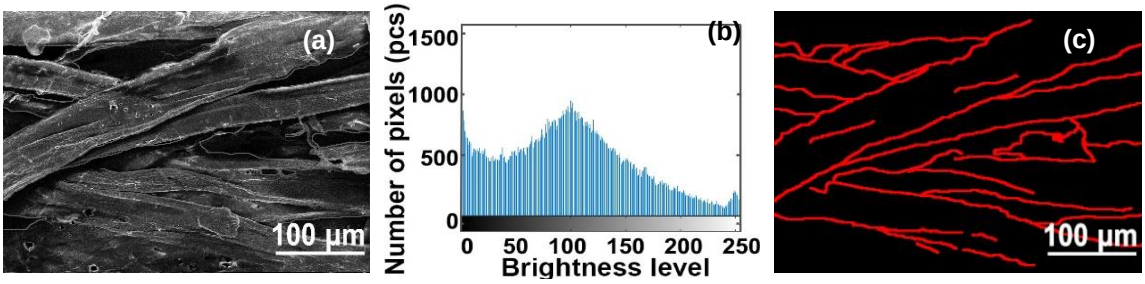

Fig. 2. SEM image processing: (a) SEM original micrograph of insulation pressboard 500x, (b) greyscale histogram, and (c) results of fibre contour image segmentation of insulation pressboard

The segmentation results of the original SEM images (Fig. 2a) using the above segmentation algorithm are shown in Fig. 2c.

Measurement Parameters

The previous study (Wang *et al.* 2020) described the method of calculating the fibre width, porosity, and other parameters using image processing, which is also applicable to the study of the deterioration of insulating paperboard in different aging states.

Fibre width

The MATLAB™ tool-kit can be used directly to measure fibre width, but this method is inaccurate. The pressboard fibre tends to curve and its thickness is unevenly distributed. Thus, the central axis method was used to measure the fibre width.

Porosity

By extracting the outline of the pores in the cross-sectional image on this side, it was possible to calculate the porosity (the proportion of the pore area in the cross-section), and the internal cross-sectional structure changes of the pressboard was analysed.

Carbonisation mark area

The extent to which the tip discharge was destructive to the pressboard was determined by considering the carbonisation mark area. In this paper, the outline of Carbonisation mark was extracted, and the area was expressed by the number of pixels.

3-D reconstruction of insulation pressboard fibre

In a previous study (Wang *et al.* 2020), the authors used a three-dimensional model to observe the degradation characteristics of fibres at different discharge stages. In the present study, the authors adopted the same method to extract the cross-sectional images of the fibre sequence to construct a 3-D model of the fibres under different aging conditions.

RESULTS AND DISCUSSION

Partial Discharge Experiment Analysis of Aged Insulation Pressboard

In the present research, the constant voltage method was used to conduct long-term pressurisation experiments on insulation pressboard with different lengths of aging. The initial discharge voltage and tolerance time of each pressboard are shown in Table 1, which demonstrates that the high temperature accelerated the aging of the insulation pressboard. As the aging of the insulation pressboard increased, the tolerance time of the test sample decreased. After 32 days of aging, the initial discharge voltage of the pressboard decreased 8.3%, and the tolerance time decreased 27.7% (compared with untreated pressboard).

Table 1. Statistical Data: Initial Discharge Voltage and Discharge Tolerance Time of Insulating Pressboard at Different Aging States

Aging Time (day)	0	2	4	8	16	32
Initial Discharge Voltage (kV)	14.4	14.5	14.3	13.9	13.4	13.2
Tolerance Time (h)	14.97	14.78	14.25	13.47	11.85	10.82

Figure 3 demonstrates the curve of the maximum PD quantity of the pressboard at different aging states with the tolerance time under the needle-plate model. In the initial

stage (1 to 4 h), the PD amount of each sample was similar. With increased pressing time, the maximum PD quantity of each sample showed an upward trend before breaking down, but the effect differed in each group of specimens. The maximum PD growth rate of samples aged for 0 to 4 days was relatively stable without much fluctuation. The discharge amount of cardboard aged for 8 to 16 days exhibited a large fluctuation in the middle of the discharge. The increase rate of discharge in 6 to 7 h was significantly higher than that in the previous period. Although the overall trend was upward, the discharge amount decreased significantly in the period 7 to 12 h. The maximum PD quantity of 32-day aged pressboard rapidly increased after 4 h, and the growth rate was much higher than that of other samples. Overall, in the initial stage of discharge, the pressboard's duration of aging had no notable effect on the maximum PD quantity, and the difference in the maximum PD quantity of each sample was small. In the middle stage of testing, the maximum PD quantity of different samples gradually varied more widely. In the later stage, on the one hand, the difference between the maximum PD of each sample increased. However, with increased aging, the maximum PD increased and breakdown occurred earlier.

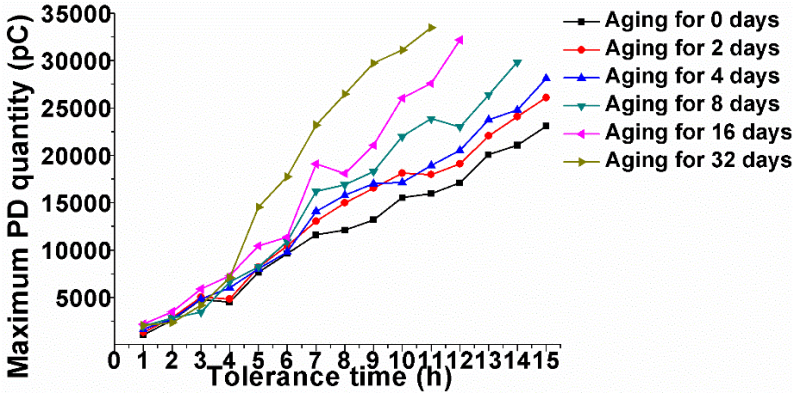

Fig. 3. Variation of maximum discharge from insulating pressboard at different aging states

Change of Fibre Width Before and After Discharge Testing of Insulation Pressboard at Different Aging States

The microstructure of insulation pressboard with different durations of aging before and after discharge testing was observed by scanning electron microscope (Figs. 4 and 5).

The image processing method introduced in the "Experimental" section was used to extract the fibre contour in different states, and the fibre width was measured. The results are illustrated in Figs. 6 and 8. The fibre width was mainly within the range between 20 μm and 44 μm, and this was divided into 14 intervals (Table 2).

Table 2. Fibre Width Intervals

Number	1	2	3	4	5	6	7	8	9	10	11	12	13	14
Width Interval (μm)	Less than 20	20 to 22	22 to 24	24 to 26	26 to 28	28 to 30	30 to 32	32 to 34	34 to 36	36 to 38	38 to 40	40 to 42	42 to 44	More than 44

The following rules were deduced from observation of the data :

(1) There were fibrils on the surface of the unaged pressboard. After 2 to 4 days of aging, the fibrils disappeared and the surface became smoother, but compared with the unaged pressboard, the whole remained neatly aligned, and the fibre width was mainly distributed between 40 and 44 μm. After PD, the rate of decrease in the fibre width of the pressboard underwent a marked change compared with that before discharge. In pressboard aged for 4 days after breakdown, the number of fibres with a width of less than 40 μm increased notably.

(2) The fibre width of 8-day-aged cardboard decreased slightly compared with that aged for 2 to 4 days. The fibres were scattered, but no obvious holes appeared on the fibre surface. After breakdown, the fibres gradually polymerised and fractured, and the width decreased to a narrow range between approximately 32 and 34 μm.

(3) After 16 days of aging, some fibres were bent and a few fibres had exfoliated, causing the roughness to increase. Most fibres were between 30 and 36 μm in width (68.1% to 81.8% of untreated cardboard). After breakdown, the fibre width was mainly distributed in the range between 24 and 26 μm (54.5% to 59.1% of untreated paperboard), and there were obvious vestiges of cauterisation visible.

(4) After 32 days of aging the cardboard, the fibre width was concentrated at approximately 30 μm, a small number of the fibres had broken, and holes appeared on the fibre surface. After the breakdown, there were almost no fibres with a width greater than 40 μm, and the proportion of fibres less than 20 μm increased notably. Fibres with a width of 24 to 26 μm accounted for the highest proportion of the total.

(5) With increased aging, the width of the fibre gradually decreased. However, after 16 to 32 days of aging, the downward trend decelerated. After PD, the fibre deterioration was noticeably worse than that before breakdown.

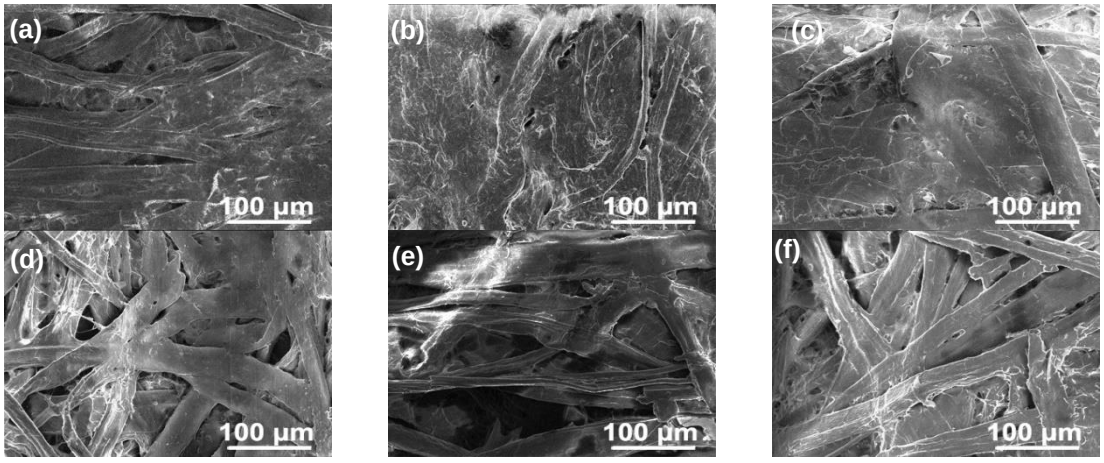

Fig. 4. Scanning electron microscopy images of insulation pressboard before discharge (500x magnification): (a) SEM image of unaged pressboard, (b) SEM image of pressboard aged 2 days, (c) SEM image of pressboard aged 4 days, (d) SEM image of pressboard aged 8 days, (e) SEM image of pressboard aged 16 days, and (f) SEM image of pressboard aged 32 days

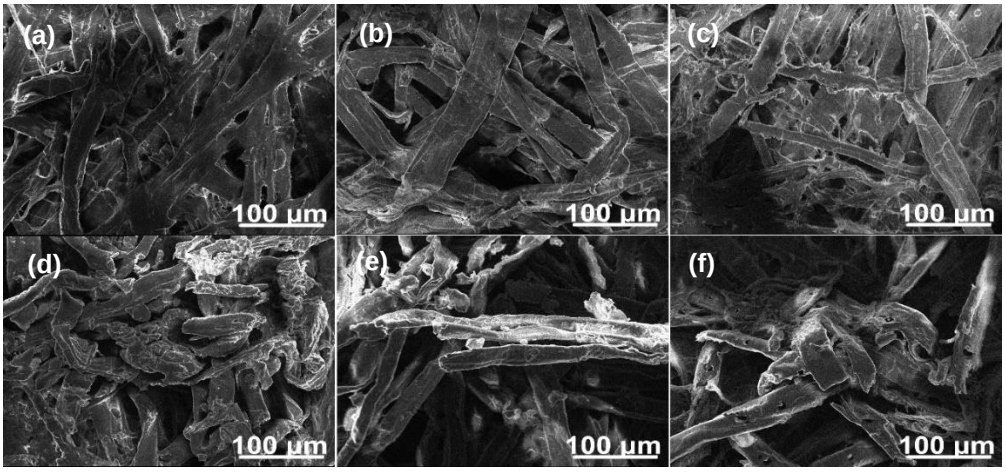

Fig. 5. Scanning electron microscopy images of insulation pressboard after discharge (500x magnification): (a) SEM image of unaged pressboard, (b) SEM image of pressboard aged 2 days, (c) SEM image of pressboard aged 4 days, (d) SEM image of pressboard aged 8 days, (e) SEM image of pressboard aged 16 days, and (f) SEM image of pressboard aged 32 days

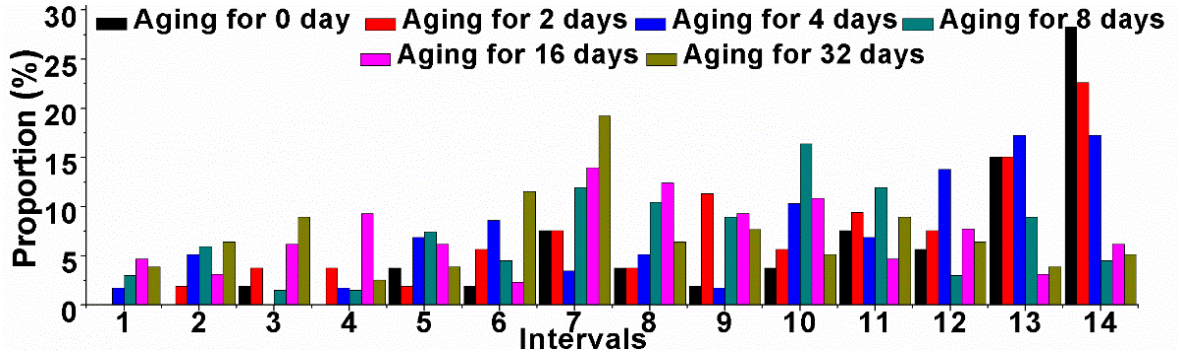

Fig. 6. Fibre width distribution of pressboard before discharge under different aging conditions

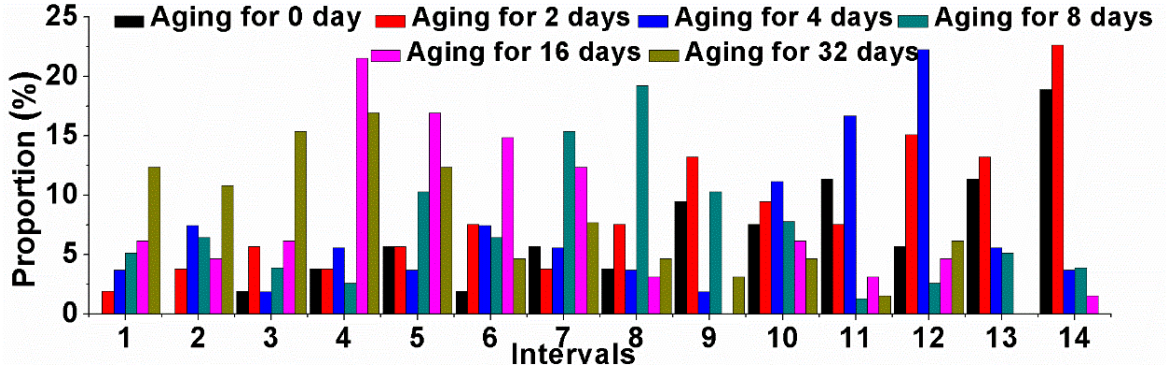

Fig. 7. Fibre width distribution of pressboard after discharge under different aging conditions

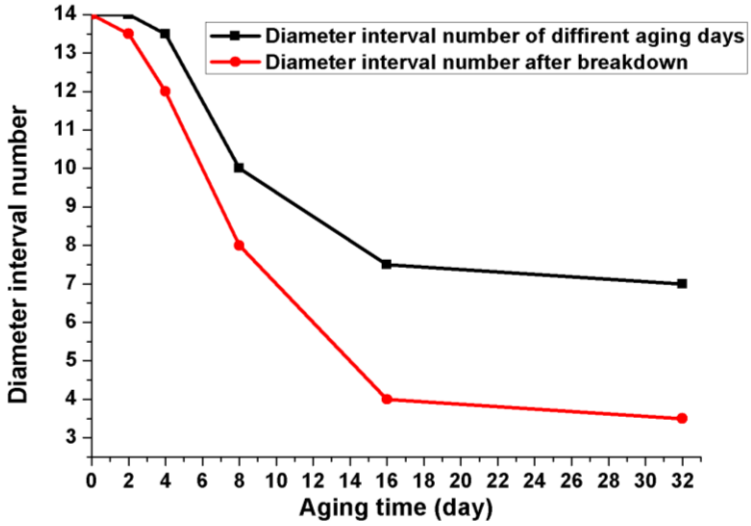

Fig. 8. Fibre width change curve of pressboard under different aging conditions

The reasons for the aforementioned rules are as follows:

(1) Under the action of thermal aging, the cell wall of fibre was severely damaged. It became thinner, displaced, and deformed. At the same time, not only the outer layer of the primary wall but also the secondary wall was broken and removed, and fibre cavities appeared, which caused fibres to split, peel, and become finer.

(2) As the aging time increased, the energy necessary to overcome thermal cracking in the oil-impregnated paper decreased, and the activation energy was reduced. Specifically, the process of changing the internal structure of the fibre accelerated, which caused the branched fibres to break, the rate of degradation of the cellulose amorphous region to increase, and the degree of destruction of the cellulose crystallisation fields to increase.

(3) PD generated high-energy particles, which continuously hit the cellulose, causing fibre ablation and acceleration of the deterioration process.

(4) During PD, the transformer oil decomposed, generating many active particles (such as CH_3, CH_2, and H) that reacted with the hydroxyl in the cellulose. These reactions formed oxides, such as ketones, aldehydes, carboxylic acids, *etc.*, resulting in weakened hydrogen bonding and reduced oxidation resistance. Meanwhile, these products formed hydronium ions. The protonation of water molecules catalysed the separation of cellulose, increasing the damage to the fibres after breakdown (their diameter also decreased notably).

Variation of Porosity Before and After Discharge Testing of Insulation Pressboard in Different Aging States

Using the porosity calculation method mentioned in the section "Porosity," the cross-section information of the paperboard was digitised. Figure 9 shows the change in cross-sectional porosity of the insulation pressboard before and after discharge testing in different states. In addition, the fibre model in each state was established by using the 3-D reconstruction technology introduced in the section "3-D reconstruction of insulation pressboard fibre," and the internal morphology of the fibre was observed (Fig. 10).

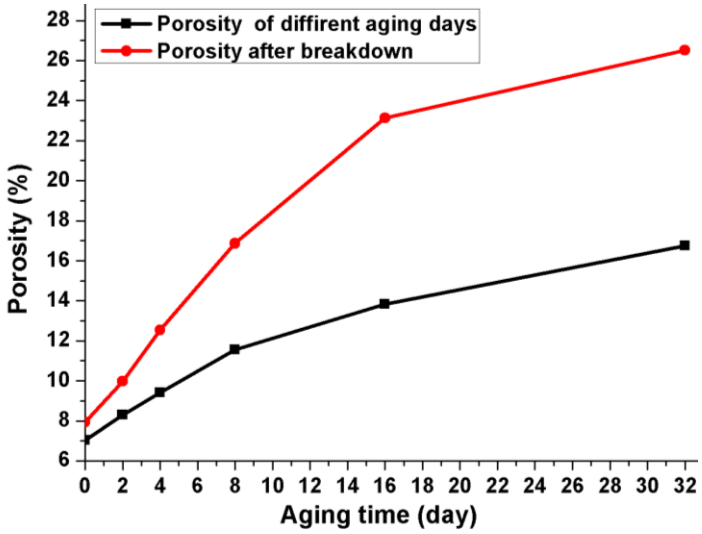

Fig. 9. Variation in porosity before and after breakdown of insulation pressboard with different durations of aging

From the analysis of the 3-D fibre model and changes in the cross-sectional porosity of the pressboard, it was determined that:

(1) The fibres inside the unaged pressboard were tightly bonded, with no obvious pores or breakage. As the aging time increased, the tightness between the fibres decreased, gaps appeared, and the arrangement of the fibres was rarefied.

(2) As the length of aging time increased, the porosity of the cardboard increased.

(3) The porosity of unaged pressboard was only 7.02%. After 16 days of thermally aging the insulating pressboard, the porosity reached 13.82%. When it was aged for 32 days, the rate rose to 16.74%.

(4) After breakdown, the fibre was more severely damaged than before discharge, and the inside was also damaged, with larger holes and cracks, and visible ablation marks. Simultaneously, the porosity rose rapidly compared with the rate before discharge, but the trend remained similar. The more aged the sample, the higher the porosity.

The reasons for the aforementioned rules are as follows:

(1) The insulation pressboard itself was porous, and it was composed of many interlaced fibres, but these interlaced fibres were not completely tightly connected and there were inevitably some pores present.

(2) The insulating paperboard is mainly composed of cellulose, hemicellulose and other components, of which cellulose accounts for the highest proportion, exceeding 90%. Due to the effect of thermal stress, cellulose and hemicellulose continue to crack. During the reaction, hemicellulose cracks and releases heat, and cellulose absorbs heat. The two react with each other. Analysis of the causes of porosity changes from the perspective of cellulose molecules. Cellulose molecules contain multiple β-D-glucopyranosyl molecules, and fibres were arranged by these different cellulose molecules. Each cellulose molecule was held together by hydrogen bonds in the hydroxyl groups (—OH) of adjacent molecules. Under the effect of thermal stress, the hexagonal ring structures of some glucose monomers were destroyed, the atomic arrangement became sparse and uneven, and discontinuous atomic bonds became commonplace, causing mutual linkage between pores. Macroscopically, the number of pores in the insulating pressboard increased, the area expanded, and the porosity increased.

(3) During PD, electrons and ions bombarded the surface of the insulating pressboard, causing the cellulose molecular chain to break.

(4) Under the action of electrical stress, aldehydes and carboxylic acids were formed in the insulation pressboard. These reactions required the consumption of hydroxyl (-OH), which was the key to the formation of hydrogen bonds in cellulose bundles. Due to the PD, the hydrogen bond force was weakened, which caused more severe damage to the arrangement of cellulose molecular chains, and resulted in a marked expansion of the pore.

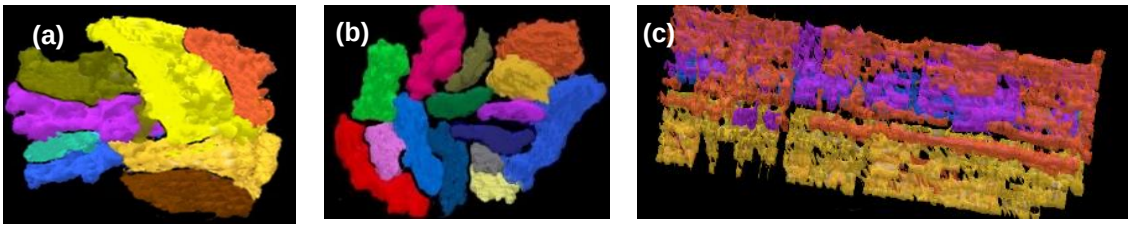

Fig. 10. A 3-D model of pressboard: (a) 3-D model of unaged pressboard, (b) 3-D model of pressboard aged for 8 days, and (c) 3-D model of pressboard after breakdown

Analysis of the Carbon Trace Area After PD of Insulation Pressboard in Different Aging States

First, the pressboard photographs were uniformly adjusted to form 2176 × 2235 × 3 RGB (red, green, and blue) images. After converting the image to greyscale, the results after breakdown of the carbon trace area of the pressboard with different durations of aging were obtained using the extraction and calculation method in Section "Carbonisation mark area," as summarised in Table 3 and Fig. 11.

The area of carbon traces of pressboard aged for 2 to 4 days was close to that of unaged pressboard. Compared with the specimens aged for 0 to 4 days, that of the 8-day-aged pressboard increased notably to 1.7 times that of the sample aged for 4 days. After 32 days of aging, the area still increased, but its rate of change decreased. These results showed that the more aged pressboard had suffered greater deterioration of its insulating properties. During the PD test, the rate of insulation deterioration with a greater durations of aging tended to increase, and the rate of development of the discharge accelerated accordingly.

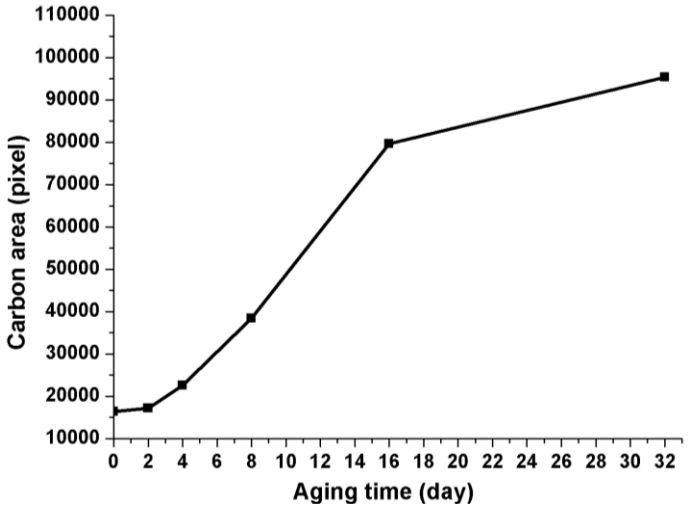

Fig. 11. Carbon trace area diagram of insulating pressboard after breakdown with different durations of aging

Table 3. Statistical Data: Carbon Trace Area of Insulating Pressboard Under Different Aging Conditions

Aging Time (day)	0	2	4	8	16	32
Area (pixel)	16348	17163	22531	38460	79659	95364
Growth Rate	/	4.9%	31.2%	70.7%	107.1%	19.7%

Based on the initial voltage, tolerance time, maximum PD, fibre width, and porosity, the reasons for the above changes were analysed as follows:

(1) Thermal aging caused the intermolecular forces of cellulose to decrease, and the fibre surface to bend and polymerise to a certain extent. Thus, the insulation performance of the paperboard decreased. However, the dielectric constant of the oil was low, and under the action of an externally applied electric field, field strength distortion occurred at fibre surface breakage. As a result, in the PD test, the initial voltage and tolerance time of the pressboard decreased by different amounts with increased aging time, and the formation of the discharge was accelerated to form a carbon trace on the pressboard more easily.

(2) Under the effect of thermal stress, the porosity of the insulating pressboard increased with the duration of aging, which exacerbated the damage caused by the PD of the insulating paperboard. At the same time, due to the increase in the number and area of pores, during the discharge process, the heat generated by the discharge decomposed the transformer oil in the interlayer pores. Gases were produced, such as H_2, CO_2, CO, low molecular weight hydrocarbon gases, and other gases that are typically associated with defective insulation. These gases increased the electric field at the pores, caused discharge to occur more easily, and increased the maximum PD during the test. Ultimately, they led to a larger area of cardboard with greater aging.

Concurrently, by comparing the carbon trace on the front with that on the back of the pressboard, it was found that the line between the breakdown points of the front and back of the pressboard was not perpendicular to the horizontal plane of the pressboard. Therefore, it was speculated that the pressboard breakdown process was mainly divided into two stages. First, during the discharge experiment process, the arc continued to appear at the tip of the needle, and accompanied by a loud discharge sound. A spark was generated on the surface of the pressboard near the tip of the needle, gradually forming carbon scars, and the surface developed into a mass. Subsequently, due to the existence of pores between the aged fibre layers, the heat generated by the discharge caused the transformer oil at the interlayer pores to decompose and produce gas. Some of the bubbles from the gas accumulated in the pores, and others overflowed near the needle tip. Nevertheless, the relative permittivity of the gas was lower than that of oil and paperboard, causing PD to occur in the air bubbles. Positive and negative charges were generated, the air bubbles became dipoles, and electrical discharge began inside the insulation pressboard. After accumulating to a certain extent, the discharge channel developed in a dendritic shape with the needle tip at its centre. Ultimately, pressboard flashover occurred.

CONCLUSIONS

1. Image processing technology was used to extract information from the image insulation pressboard. The information included fibre width, cross-section porosity, and carbon trace area. This additional data enabled accuracy in calculating the pressboard microscopic parameters.
2. Through continuous cross-sectional images and three-dimensional reconstruction technology, a fibre model was constructed. The microscopic results indicated that thermal aging and PD destroyed the surface morphology of the fibre in the pressboard. When the aging time was longer, damage to the fibre morphology was more serious. Aging of the pressboards destroyed the fibre flatness, reduced the fibre width, and decreased the compactness. With an increased aging time, the number of holes in the fibres increased, and the fibre breaks and tears, resulted in decreases in the mechanical properties and insulation strength of the pressboard.
3. Thermal aging damaged the cell wall, thus accelerating the decomposition of fibres and promoting the breakage of fibre chains. As the aging time increased, the fibre width gradually decreased. After 16 days of aging, the fibre width was mainly concentrated in the range of 68.1% to 81.8% that of unaged pressboard, and the rate of fibre thinning tended to a constant value when aged between 16 to 32 days. After PD, the fibres cracked due to ablation, and the fibre width decreased rapidly. After 32 days of aging pressboard breakdown, the fibre width was concentrated between 22 and 26 μm.
4. Thermal aging destroyed the insulating properties of pressboard. Under the action of thermal stress, the cellulose hydrogen bond was broken, which affected the structural and mechanical properties of the insulating pressboard. With increased aging, the tightness of the interlayer bond decreased, and the number of interlayer holes and the volume of the fibre were positively correlated with the duration of aging. When the pressboard was aged for 16 days, the porosity reached 13.83%. When the pressboard was aged for 32 days, the porosity reached 16.74%, which was 2.38 times of that of the insulating pressboard. After PD, the electric field at the pores was strong, which accelerated the discharge process and intensified the damage to the pressboard.
5. As the aging of the insulating pressboard increased, its fibre structure was destroyed, and the insulating performance reduced. As a result, pressboard insulation discharge tolerance times gradually shortened, the initial discharge voltage showed a downward trend, and, after breakdown, a carbon trace on the surface of the pressboard area formed rapidly. Combined with the changes in peak discharge in each state of aging, it was shown that the more rapidly the aging insulation pressboard discharge developed, the more obvious the damage caused by partial discharge.

REFERENCES CITED

Carrascal, I. A., Fernández-Diego, C., Casado, J. A., Diego, S., Fernández, I., and Ortiz, A. (2018). "Quantification of kraft paper ageing in mineral oil impregnated insulation systems through mechanical characterization," *Cellulose* 25(6), 3583-3594. DOI: 10.1007/s10570-018-1788-1

Darveniza, M., Saha, T. K., Hill, D. J. T., and Le, T. T. (1992). "Study of degradation of cellulosic insulation materials in aged power transformers by electrical and chemical techniques," in: *Proceedings of the Electric Energy Conference*, Brisbane, Australia, pp. 299-305.

Du, H., Chen, X., and Xi, J. (2019). "An improved background segmentation algorithm for fringe projection profilometry based on Otsu method," *Optics Communications* 453, 810-818. DOI: 10.1016/j.optcom.2019.06.044

Emsley, A. M., Heywood, R. J., Ali, M., and Eley, C. M. (1997). "On the kinetics of degradation of cellulose," *Cellulose* 4(1), 1-5. DOI: 10.1023/A:1018408515574

Joshi, A., and Bhanot, V. (2005). "Effect of accelerated aging on the tensile index of a synthetic insulation paper," *NDT & E International* 38(5), 394-396. DOI: 10.1016/j.ndteint.2004.11.001

Joshi, A., Kumar, S., and Verma, N. K. (2006). "Study of dispersion, absorption and permittivity of an synthetic insulation paper—with change in frequency and thermal aging," *NDT & E International* 39(1), 19-21. DOI: 10.1016/j.ndteint.2005.05.004

Kim, S., E., Jeon, J., J., and Eom, I., K. (2016). "Image contrast enhancement using entropy scaling in wavelet domain," *Signal Process* 127, 1-11. DOI: 10.1016/j.sigpro.2016.02.016

Li, G., Li, L., Wang, Y., and Zhang, R. (2017). "Research on changes of oil moisture, acid value, furfural and insulation paper polymerization degree of oil-paper insulation under accelerated thermal aging," in: *Proceedings of the 5th International Conference on Mechatronics*, Chongqing, China, pp. 1391-1397. DOI: 10.2991/icmmcce-17.2017.244

Liao, R. J., Tang, C., Yang, L. J., and Grzybowski, S. (2008). "Thermal aging micro-scale analysis of power transformer pressboard," *IEEE Transactions on Dielectrics and Electrical Insulation* 15(5), 1281-1287. DOI: 10.1109/tdei.2008.4656235

Liao, R. J., Yan, J., M., Yang, L., J., Zhu, M., Z., and Sun, C., X. (2011). "Characteristics of partial discharge-caused surface damage for oil impregnated insulation paper," *Proc CSEE* 31, 129-137.

Lundgaard, L. E., Hansen, W., Linhjell, D., and Painter, T. J. (2004). "Aging of oil-impregnated paper in power transformers," *IEEE Trans. Power Deliv.* 19(1), 230-239. DOI: 10.1109/TPWRD.2003.820175

Mariprasath, T., and Kirubakaran, V. (2018). "A real time study on condition monitoring of distribution transformer using thermal imager," *Infrared Physics & Technology* 78-86. DOI: 10.1016/j.infrared.2018.02.009

Otsu, N. (1979). "A threshold selection method from gray-level histograms," *IEEE Transactions on Systems Man. & Cybernetics* 9(1), 62-66. DOI: 10.1109/TSMC.1979.4310076

Pirie, H., Liu, Y., Soumyanarayanan, A., Chen, P., He, Y., and Yee, M. M. (2020). "Imaging emergent heavy Dirac fermions of a topological Kondo insulator," *Nature Physics* 16(1). 52-56. DOI: 10.1038/s41567-019-0700-8.

Tu, Y., Chen, J., Wang, S., and Wang, W. (2016). "Moisture migration in oil-impregnated film insulation under thermal ageing," *IEEE on Dielectrics and Electrical Insulation* 23(2), 1135-1141. DOI: 10.1109/TDEI.2015.005406

Wang, L., Tang, C., Zhu, S., and Zhou, S. (2018a). "Terahertz time domain spectroscopy of transformer insulation paper after thermal aging intervals," *Materials* 11(11), Article number 2124. DOI: 10.3390/ma11112124

Wang, Y., Fei, R., Feng, C., and Fang, S. (2020). "Failure modes of insulating pressboard subjected to high electric fields and durations: Evidence of partial discharge and changes at the microscopic scale," *BioResources* 15(2), 3585-3603. DOI: 10.15376/biores.15.2.3585-3603

Wang, Y., Luo, Y., Guan, J., and Ding, R. (2019a). "Dielectric properties of epoxy resin impregnated paper insulation in different stages of partial discharge development," *Polymer Composites* 41(1), 360-368. DOI: 10.1002/pc.25375

Wang, Y., Luo, Y., Wang, Y., and Fei, R. (2019b). "Partial discharge damage mechanisms in laminated oil-paper insulation," *Cellulose* 26, 5707-5718. DOI: 10.1007/s10570-019-02470-5

Wang, Y., Wang, Y., and Jiang, X. (2018b). "The microscopic morphology of insulation pressboard: An image processing perspective," *Cellulose* 25(5), 3051-3065. DOI: 10.1007/s10570-018-1768-5

Yan, J., Liao, R., Yang, L., and Li, J. (2012). "Study on microstructure and electrical properties of oil-impregnated paper insulation after exposure to partial discharge," *European Transactions on Electrical Power* 22(6), 733-746. DOI: 10.1002/etep.600

Yan, J., Liao, R., Yang, L., Hao, J, and Sun, C., X. (2011). "Analysis of damage products of oil-impregnated insulation paper caused by partial discharge," *Trans. Chin. Electrotech. Soc.* 26(5), 184-191+198. DOI: 10.3354/cr00999

Zhou, L., J., Wang, D., Y., Guo, L., Wang, L., J., Jiang, J., f., and Liao, W. (2017). "FDS analysis for multilayer insulation paper with different aging status in traction transformer of high-speed railway," *IEEE Transactions on Dielectrics and Electrical Insulation* 24, 3236-3244. DOI: 10.1109/TDEI.2017.006547

Article submitted: April 30, 2020; Peer review completed: June 4, 2020; Revised version received and accepted: July 14, 2020; Published: July 6, 2020.
DOI: 10.15376/biores.15.3.6442-6456